Localization in one-dimensional chains with Lévy-type disorder

Sepideh S. Zakeri,[1,*] Stefano Lepri,[2,3,†] and Diederik S. Wiersma[1,4,5]

[1]*European Laboratory for Non-linear Spectroscopy (LENS), University of Florence, Via Nello Carrara 1, I-50019 Sesto Fiorentino, Italy*

[2]*Consiglio Nazionale delle Ricerche, Istituto dei Sistemi Complessi, via Madonna del Piano 10, I-50019 Sesto Fiorentino, Italy*

[3]*Istituto Nazionale di Fisica Nucleare, Sezione di Firenze, via Giovanni Sansone 1, I-50019 Sesto Fiorentino, Italy*

[4]*Consiglio Nazionale delle Ricerche, Istituto Nazionale di Ottica, Largo Fermi 6, I-50125 Firenze, Italy*

[5]*Universitá di Firenze, Dipartimento di Fisica e Astronomia, via Giovanni Sansone 1, I-50019 Sesto Fiorentino, Italy*

(Received 8 December 2014; published 6 March 2015)

We study Anderson localization of the classical lattice waves in a chain with mass impurities distributed randomly through a power-law relation $s^{-(1+\alpha)}$ with s as the distance between two successive impurities and $\alpha > 0$. This model of disorder is long-range correlated and is inspired by the peculiar structure of the complex optical systems known as Lévy glasses. Using theoretical arguments and numerics, we show that in the regime in which the average distance between impurities is finite with infinite variance, the small-frequency behavior of the localization length is $\xi_\alpha(\omega) \sim \omega^{-\alpha}$. The physical interpretation of this result is that, for small frequencies and long wavelengths, the waves feel an effective disorder whose fluctuations are scale dependent. Numerical simulations show that an initially localized wave-packet attains, at large times, a characteristic inverse power-law front with an α-dependent exponent which can be estimated analytically.

DOI: 10.1103/PhysRevE.91.032112 PACS number(s): 05.60.Cd, 05.45.−a, 42.25.Dd, 63.20.Pw

I. INTRODUCTION

The spatial distribution of disorder plays a key role on transport properties in disordered media, allowing anomalous laws like superdiffusion to arise. This interesting topic has been the basis of numerous theoretical and experimental studies in a wide variety of complex systems. Recently, one of the studies reported on the realization of some engineered materials named Lévy glasses in which light rays propagate through an assembly of transparent microspheres embedded in a scattering medium [1]. If the diameter of the microspheres ϕ is designed to have a power-law distribution $p(\phi) \sim \phi^{-(\alpha+1)}$, where α is the so-called Lévy exponent defining the degree of the heterogeneity of the system, light can indeed perform superdiffusion. Although a random-walk model is rich and precise to describe light transport through Lévy glasses and successfully explains the experimental observations [2], it cannot address wave properties such as polarization and interference. Therefore, an open question to understand is how the interference of waves can affect the propagation and what might be the possible role of Anderson localization [3,4] in such materials.

Although our main motivation stems from the above described setup, it is worth mentioning some related studies of systems with Lévy-type disorder that include transport in quantum wires [5], photonic heterostructures [6], and disordered electronic systems [7,8]. The purpose of this work is to provide a framework to investigate localization in power-law correlated disordered systems and to illustrate how the localization length is affected by different characteristic features of the system such as frequency, degree of heterogeneity, disorder strength, etc. To address the above issues, we consider a very simple model, a harmonic chain of coupled oscillators with random impurities separated by random distances s having a power-law distribution $p(s) \propto s^{-(\alpha+1)}$. This model of disorder is clearly inspired by the peculiar structure of Lévy glasses. As usual, the one-dimensional case allows for a detailed study. In particular, the Lyapunov exponent $\gamma(\omega)$, the inverse of the frequency-dependent localization length $\xi(\omega) = \gamma(\omega)^{-1}$, can be computed straightforwardly. Our main result is that, in the small-frequency regime, the scaling relation $\gamma(\omega) \propto \omega^\alpha$ is numerically estimated for the Lyapunov exponent in the range $1 \leqslant \alpha \leqslant 2$, i.e., when the variance of the distances $\langle s^2 \rangle$ is infinite. Instead, for $\alpha > 2$, the usual scaling $\gamma(\omega) \propto \omega^2$, typical of random uncorrelated disorder [9] is recovered.

The model and some theoretical arguments, based on the Hamiltonian map formulation of the transfer method, are presented in Sec. II. We then present and discuss the complete numerical steady-state analysis in Sec. III of this paper. For a more comprehensive understanding of the transport in such disordered media, we investigate and report in Sec. IV the time evolution of an initially localized wave packet. In particular, we consider the time- and disorder-averaged energy profile $\langle \overline{e_n(t)} \rangle$. Here we show that in the range $1 \leqslant \alpha < 2$, the asymptotic tails of the energy profile decay with an α-dependent power-law exponent. In contrast, for the range $\alpha \geqslant 2$, depending on the type of the initial excitation, the power-law exponent is independent of α. Moreover, we pay close attention to the time evolution of the different moments $m_\nu(t)$ of the $\langle \overline{e_n(t)} \rangle$ and discuss the α-dependent properties in the range $1 \leqslant \alpha < 2$. Finally, we summarize our results in the concluding Sec. V.

II. THEORETICAL DESCRIPTION

A. Model: One-dimensional Lévy-type disordered lattice

We considered a one-dimensional harmonic disordered lattice of n sites with masses m_n. The governing equations of motion are

$$m_n \ddot{u}_n = k(u_{n+1} - u_n) + k(u_{n-1} - u_n), \tag{1}$$

*zakeri@lens.unifi.it

†stefano.lepri@isc.cnr.it

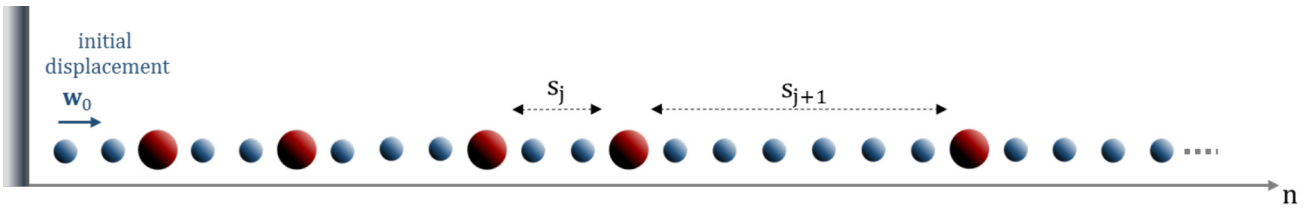

FIG. 1. (Color online) Schematic illustration of the model used to study localization in a one-dimensional lattice with Lévy-type disorder. Small blue balls represent the background mass of the lattice m and large red balls are the defects with mass M distributed on the lattice through a power-law relation $p(s) \propto s^{-(\alpha+1)}$, where s is the number of lattice sites between two successive defects and the index $j = 1, \ldots, N_d$. An initial displacement $\mathbf{w}_0$ is given to the first site of the lattice to initiate iteration of the transfer matrix over the entire lattice.

where k is spring constant ($k \neq 0$), u_n is displacement of the nth site of the lattice from its equilibrium position, and $n = 1,2,\ldots,N$.

In the present work, we consider dichotomic disorder whereby m_n assumes two possible values, either m as the background mass of the lattice or M to represent mass of the defects. Illustrated in Fig. 1, disordered lattices of length N were constructed by arrangement of N_d defects through a power-law distribution $p(s) \propto s^{-(\alpha+1)}$, where s was the random number of lattice sites with mass m between two successive defects. As a direct consequence of such choice of $p(s)$, the mass of the entire lattice was the parameter with α-dependent statistical properties. Obviously, its average density can be written as

$$\langle m \rangle = \rho M + (1-\rho)m, \tag{2}$$

where $\rho = \frac{N_d}{N}$ is the fraction of defects on the lattice. In the range $1 \leqslant \alpha < 2$, $\langle \rho \rangle$ is finite. On the other hand, for $\alpha < 1$, ρ vanishes in the thermodynamic limit $N \to \infty$ since the average distance between consecutive defects diverges in this regime. In this paper, we mainly focus on the case $\alpha > 1$ (in which $\langle s \rangle$ is finite) and will comment only briefly on the case $\alpha < 1$, which is somehow more peculiar.

Before proceeding, we recall that random walks on such class of Lévy structures have been thoroughly studied in a series of recent papers [10–15] as a minimal model that includes quenched disorder and anomalous diffusion. Depending on the value of α, fundamentally different regimes of transport are achieved: Indeed, walkers superdiffuse for $\alpha < 1$. Several distinguished features of the quenched nature of disorder, like the importance of initial conditions and the consequences on higher-order statistics of the diffusive process, are discussed in the above mentioned papers. It can be thus envisaged that also localization properties may display unusual features.

B. Statistical properties of the disorder

Using the algorithm described in [16], positive integer power-law random numbers were generated to construct disordered lattices. For a preliminary statistical characterization, we computed the ensemble-averaged power spectrum,

$$S(k) = \frac{1}{N}\left\langle \left| \sum_{n=1}^{N} m_n \exp(-ikn) \right|^2 \right\rangle, \tag{3}$$

where the average is over different realization of the disorder. The low-wave-number behavior of S provides information on the large-scale decay law of the disorder correlation function which will be necessary for the subsequent analysis. Figure 2 indicates that, for $\alpha < 2$, S has a power-law singularity $|k|^{-\Theta}$ for small k. This implies that the disorder correlation is indeed decaying as an inverse power of the relative distance with an exponent $1 - \Theta$. The exponent will be important in the subsequent analysis: Fitting of the numerical data suggests the following relation with the Lévy parameter α (see the inset of Fig. 2):

$$\Theta(\alpha) = \begin{cases} \alpha, & \text{if} \quad 0 < \alpha < 1, \\ 2 - \alpha, & \text{if} \quad 1 < \alpha < 2. \end{cases} \tag{4}$$

A theoretical justification of the above relation can be given based on the similarity of this process with the correlation of a Lévy walk as discussed by Geisel in Ref. [17]. Note that in all the examined cases $\Theta < 1$, so the power spectrum is integrable and the associated process can be considered as stationary for any α.

For what concerns the dependence on the lattice size (data not shown), by comparing data for different lengths, we

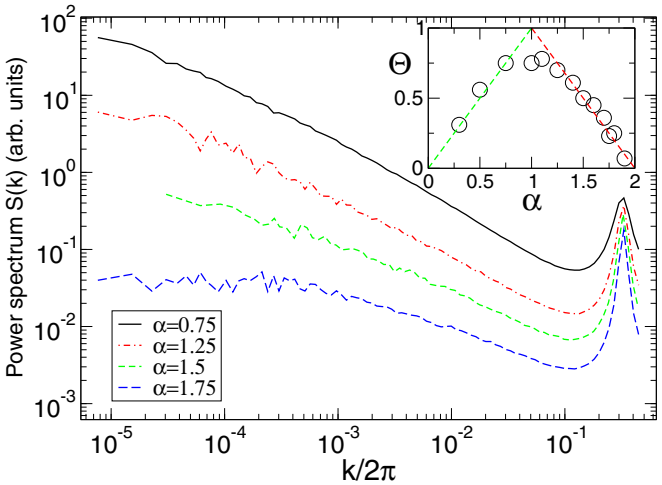

FIG. 2. (Color online) Power spectra, Eq. (3), for different values of the exponent α; each spectrum is obtained for sequences of length 2^{17} over an ensemble of 10^4 realizations. The inset shows the dependence of the exponent of the small-frequency singularity $|k|^{-\Theta}$ on α.

found that for $\alpha > 1$ the spectra are N independent, while for $\alpha < 1$ the spectra decrease with increasing N roughly like $N^{\alpha-1}$. This is because the density of defects vanishes in the thermodynamic limit and almost-ordered realizations dominate the statistical averages.

To conclude this section, let us mention that a similar model has been studied in Ref. [18] (see also the related work [19]). The main differences with our work is that the sequence of masses is generated as a trace of a fractional Brownian motion that, by construction, has also a a power-law singularity at small wave number. It was there shown that in the nonstationary case ($\Theta > 1$ in our notation), a mobility edge can exist at a finite frequency value.

C. Transfer matrix approach

As is well known, the localization properties can be studied by the transfer matrix method [20]. Assuming that u_n oscillates harmonically in time at an angular frequency ω, so that $u_n = v_n e^{i\omega t}$, Eq. (1) can be written as an eigenvalue problem,

$$-m_n\omega^2 v_n = k(v_{n+1} - v_n) + k(v_{n-1} - v_n), \tag{5}$$

that, upon defining

$$\boldsymbol{w_n} \equiv \begin{pmatrix} v_n \\ v_{n-1} \end{pmatrix}; \quad \boldsymbol{T_n} \equiv \begin{pmatrix} 2 - m_n\omega^2/k & -1 \\ 1 & 0 \end{pmatrix},$$

for $n = 2,3,\ldots,N-1$ can be recast in the form

$$\boldsymbol{w_{n+1}} = \boldsymbol{T_n}\boldsymbol{w_n}, \tag{6}$$

where T_n is a 2×2 transfer matrix of the nth site on the lattice. By iteration of the transfer matrix over the entire lattice and applying the appropriate boundary conditions of the system, solutions of Eq. (5) as a function of frequency ω can be obtained.

The central quantity to be computed is the Lyapunov exponent $\gamma(\omega)$, which gives the inverse of the localization length $\xi(\omega)$. It is convenient to define a new parameter $R_n = v_n/v_{n-1}$. Inserting R_n into Eq. (5), one obtains the following recursive relation [21]

$$R_{n+1} = 2 - \frac{m_n\omega^2}{k} - \frac{1}{R_n}. \tag{7}$$

Equation (7) can be interpreted as a "discrete time" stochastic equation. The mass m_n plays the role of a noise source (with bias) whose strength is gauged by the frequency ω. In the present model, the Lyapunov exponent $\gamma(\omega)$ as the inverse of localization length can be computed by

$$\xi(\omega)^{-1} = \gamma(\omega) = \langle \ln R_n \rangle. \tag{8}$$

Also the integrated density of states $I(\omega)$ follows from node counting arguments, i.e., $I(\omega) = f$, where f is the fraction of negative R_n values.

For deeper analysis of the systems of interest, let us rewrite Eq. (5) in a different notation; introducing the new variables $q_n = v_n$ and $p_n = q_n - q_{n-1}$, the transfer map can be reformulated as follows. Letting $\omega^2 m_n = \Omega^2(1+\mu_n)$, $\Omega^2 = \omega^2\langle m\rangle$, and $\mu_n = m_n/\langle m\rangle - 1$ is a zero-average random variable and $\langle \mu^2 \rangle$ is finite at least for $\alpha > 1$. Plugging q_n and p_n into Eq. (5) and setting $k = 1$, one finds the following two-dimensional map [22]:

$$p_{n+1} = p_n - \Omega^2(1+\mu_n)q_n, \tag{9}$$

$$q_{n+1} = q_n + p_{n+1}. \tag{10}$$

The following transformation relations can be introduced by using the canonical variables (r_n,θ_n), where r_n and θ_n are amplitude and phase of the eigenvector at site n, respectively,

$$p_n = \sqrt{2\Omega}\, r_n \sin\theta_n; \quad q_n = \sqrt{\frac{2}{\Omega}}\, r_n \cos\theta_n. \tag{11}$$

Substituting Eqs. (11) back into Eqs. (9) and (10) and neglecting terms of the order Ω^2 and higher, one then obtains the following map:

$$\left(\frac{r_{n+1}}{r_n}\right)^2 = 1 - \mu_n\Omega\sin 2\theta_n + O(\Omega^2), \tag{12}$$

$$\tan\theta_{n+1} = \tan(\theta_n - \Omega) - \Omega\mu_n. \tag{13}$$

Equation (13) describes the evolution of the phase as it is perturbed by disorder and can be approximated as [23]

$$\theta_{n+1} = \theta_n - \Omega + \Omega\mu_n \sin^2\theta_n. \tag{14}$$

Long-range correlations of μ_n lead to subdiffusive phase fluctuations. Within the same approximation, the Lyapunov exponent is obtained by expanding the logarithm

$$\gamma = \frac{1}{2}\left\langle \ln\left(\frac{r_{n+1}}{r_n}\right)\right\rangle \approx -\frac{1}{2}\Omega\langle\mu_n \sin 2\theta_n\rangle + \frac{1}{4}\Omega^2\langle\mu_n^2 \sin^2 2\theta_n\rangle + \cdots. \tag{15}$$

The main issue is to estimate the correlators in Eq. (15). Following the same path as in Ref. [23] [see, in particular, Sec. (5.2)], it can be shown that

$$\langle\mu_n \sin 2\theta_n\rangle = 2\Omega\sum_{m=1}^{\infty}\langle\mu_n\mu_{n-m}\rangle\cos(2\Omega m), \tag{16}$$

$$\langle\mu_n^2 \sin^2 2\theta_n\rangle \approx \tfrac{1}{2}\langle\mu_n^2\rangle. \tag{17}$$

We thus obtain

$$\gamma = \frac{1}{8}\Omega^2\langle\mu_n^2\rangle\left[1 + 2\sum_{m=1}^{\infty}\frac{\langle\mu_n\mu_{n-m}\rangle}{\langle\mu_n^2\rangle}\cos(2\Omega m)\right]. \tag{18}$$

Note that this formula agrees with the long-wavelength limit of Eq. (22) in [24], which was obtained for weak disorder (where $\Omega \approx k$). The sum is basically the Fourier transform of the correlation function, i.e., the power spectrum of the sequence of masses studied above. We thus expect three cases.

(i) For short-range correlations as in the case $\alpha > 2$, the second term in Eq. (18) is finite and independent of the frequency. So it just provides a proportionality constant. The Lyapunov exponent is thus expected to scale, up to some constant prefactor as in the standard uncorrelated case [9],

$$\gamma(\omega) \propto \omega^2\frac{\langle m^2\rangle - \langle m\rangle^2}{8\langle m\rangle}. \tag{19}$$

(ii) For long-range correlations and in the case $1 < \alpha < 2$, the fluctuation spectrum diverges at small frequencies so the second term in Eq. (18) dominates so that

$$\gamma \sim \Omega^2 S(2\Omega). \tag{20}$$

Using the result [Eq. (4)] that the spectrum goes as $k^{\alpha-2}$ and recalling the definition of Ω, this means that the Lyapunov exponent should be proportional to ω^α.

(iii) Furthermore, if we assume that the same argument holds also for $\alpha < 1$, we may conclude that $\gamma \sim \omega^{2-\alpha}/N^{1-\alpha}$, which means that γ vanishes for $N \to \infty$. This argument may not be entirely correct since, in this case, $\langle \mu_n^2 \rangle$ also vanishes.

To conclude this section, we mention that John and Stephen [25] studied a related model of a classical wave in the continuum limit where the mass fluctuations μ were quenched random variables but power-law correlated in space $\langle \mu(x)\mu(x') \rangle \sim (x - x')^{-2m}$. According to their Eq. (7.5), in one dimension the Lyapunov exponent should be

$$\gamma(\omega) \sim \begin{cases} \omega^2 & \text{if } m > 1/2, \\ \omega^{\frac{1}{1-m}} & \text{if } m < 1/2. \end{cases} \tag{21}$$

Although the models are pretty similar at large scales, our result is different from this last estimate. The origin of the discrepancy is not clear at this stage; however, it is true that the approach in Ref. [25] relies on some approximate self-consistent calculations while the calculations reported here are asymptotically exact.

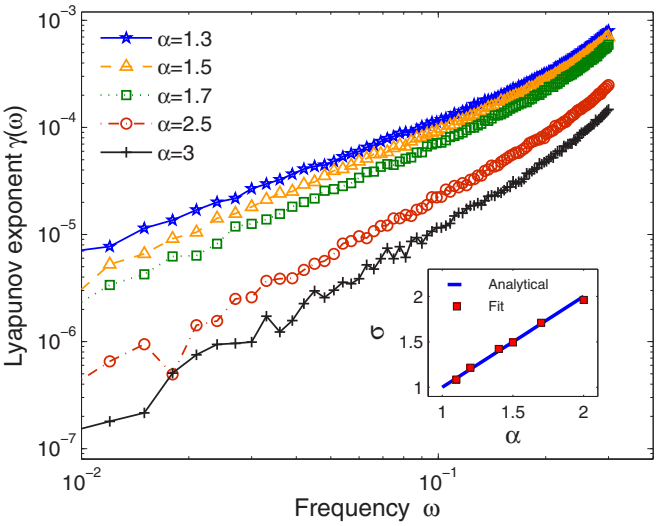

FIG. 3. (Color online) Variations of the Lyapunov exponent $\gamma(\omega)$ versus ω for systems with different α parameter, setting $N_d = 5 \times 10^6$, $M/m = 3$, and $k = 1$. Lyapunov exponents were normalized after $N_{it} = 5 \times 10^4$ iterations of the transfer matrix. Frequency ω was varied from 0.01 to 0.3. The inset shows the scaling exponent σ [of the frequency-dependent Lyapunov exponent $\gamma(\omega) \approx \omega^\sigma$] versus α. Numerical results for the scaling are obtained by power-law fits on the data set for Lyapunov exponent and an excellent agreement is obtained with the theoretical predictions $\gamma(\omega) \approx \omega^\alpha$ in the low-frequency regime for the range $1 < \alpha < 2$.

III. NUMERICAL RESULTS

In this section, numerical results of the model described in the previous section are presented. We have carefully studied the dependence of the Lyapunov exponent on different characteristic parameters of the systems. Data analysis was performed mainly for systems with $1 \leqslant \alpha < 2$, however, some computations were done for systems with $\alpha \geqslant 2$ to allow comparison of the behaviors in two different transport regimes. Throughout the rest of the paper, the spring constant was assumed to be $k = 1$ and, unless otherwise stated, the mass ratio was fixed to $M/m = 3$.

A. Lyapunov exponent

According to the definition described in Eq. (8), the Lyapunov exponent is the exponential growth or decay rate of a vector in the limit $N \to \infty$.

Due to the long-range spatial correlations (especially in the regime $1 \leqslant \alpha < 2$), the convergence of the numerical value of γ could vary from a single realization to another and usually requires a long series of iterations. In order to ensure that our obtained results were independent of the disorder realization (i.e., that self-averaging holds), a series of lattices with a different number of defects N_d were studied and compared. Results led us to the conclusion that for $N_d \geqslant 2 \times 10^6$, fluctuations of $\gamma(\omega)$ versus N_d are relatively small (better than $\simeq \pm 13\%$) in the systems with different α parameters. Clearly, as α approaches 2, even smaller values of N_d can yield a fast convergence $\gamma(\omega)$. However, to improve stability of our results even further, $N_d = 5 \times 10^6$ defects were used to construct our desired disordered systems. We pursue this number consistently in the rest of this paper for the analysis of very large lattices (asymptotic limit). In all the studied cases, the same initial displacement $\mathbf{w_0}$ must be assigned to start iteration of the transfer matrix. Note that Lyapunov exponent has this intrinsic property to be independent of $\mathbf{w_0}$ and our numerical results were in excellent agreement with that.

Since we mostly focus on the behavior of the Lyapunov exponent in the small frequency regime, we first checked that in all the presented cases the integrated density of states is linearly changing with the frequency, $I(\omega) \sim \omega$. The physical interpretation of this fact is simply that the spectrum is effectively equivalent to an ordered chain with a renormalized wave speed.

In Fig. 3, variations of the Lyapunov exponent $\gamma(\omega)$ versus frequency ω for systems with different α parameter are shown in doubly logarithmic scale. In each system, as the frequency was increased from 0.01 to 0.3, greater values were obtained for the Lyapunov exponent and, accordingly, localization length was decreased. As illustrated in the inset of Fig. 3, the scaling relation predicted in the previous section is in excellent agreement with the data obtained by power-law fitting on the small-frequency region of the curves. In some cases, we also checked that the fit that includes the leading order correction ω^2 follows the data in the whole range, giving further support to the theoretical arguments above.

Another interesting physical effect that should be assessed is the dependence of the Lyapunov exponent on disorder strength or, equivalently, mass ratio M/m in our model. In an intuitive picture, one expects that higher mass ratio leads to stronger disorder, shorter localization length, and

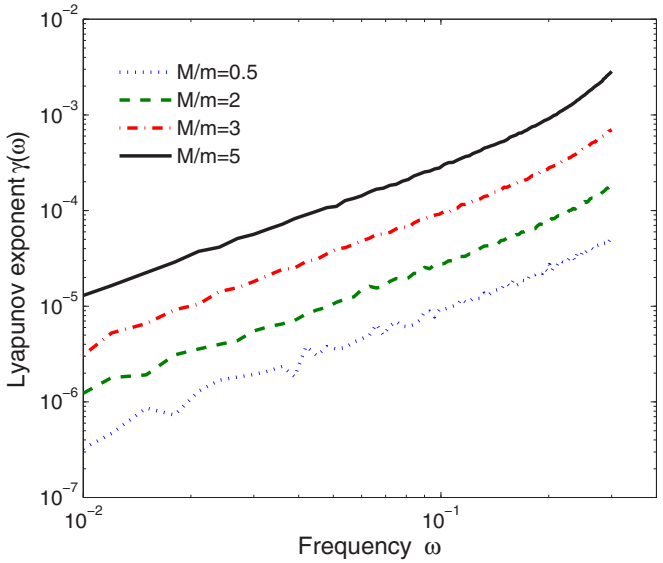

FIG. 4. (Color online) Comparison of the Lyapunov exponent $\gamma(\omega)$ versus ω for systems with $\alpha = 1.5$ and $N = 14\,648\,365$ but different mass ratios M/m. Other parameters such as N_d, N_{it}, and the frequency range are the same as those used to generate Fig. 3.

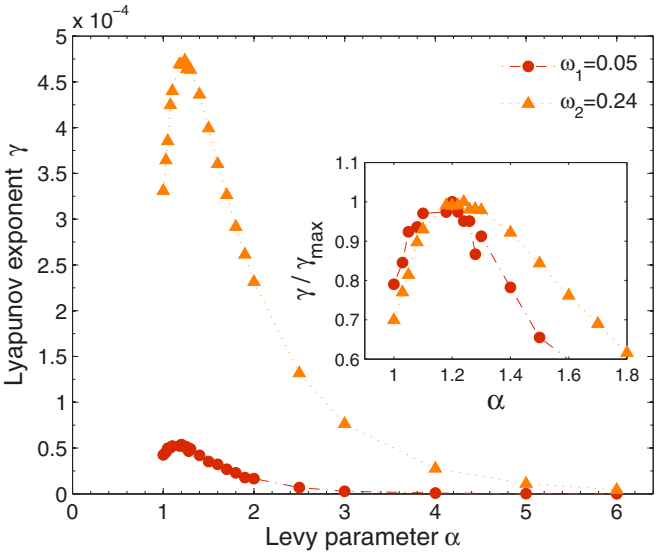

FIG. 5. (Color online) Dependence of the Lyapunov exponent on the Lévy exponent α at two fixed frequencies $\omega_1 = 0.05$ (red circles) and $\omega_2 = 0.24$ (orange triangles). The inset shows that by increasing the frequency, the peak of the Lyapunov exponent is shifted to right. For better illustration, the two curves are normalized by their maxima.

thereby greater Lyapunov exponents. In addition to that, the scaling of $\gamma(\omega) \propto \omega^{\sigma}$ intrinsically depends on transport properties of the system and hence should be independent of the mass ratio. In other words, the mass ratio should, at most, change the prefactor in the above scaling relation. To confirm this prediction, four different mass ratios, $M/m = 0.5,2,3,5$, were considered in a system with $\alpha = 1.5$ and length $N = 14\,648\,365$ composed of $N_d = 5 \times 10^6$ defects. As shown in Fig. 4, scaling of the Lyapunov exponent with frequency ω (slope of the curves) is independent of the mass ratios. However, larger values of M/m yield an increase in the Lyapunov exponent by orders of magnitude, indicating that the prefactor changes rapidly with M/m.

Figure 5 shows and compares dependence of the Lyapunov exponent on the Lévy exponent α at two fixed frequencies, $\omega_1 = 0.05$ and $\omega_2 = 0.24$. Upon decreasing α, γ was initially increased. This is in agreement with the intuition that the localization is enhanced by increasing fluctuations of the distances between defects. However, by approaching $\alpha = 1$, γ started decreasing and a peak was observed in both curves. We can therefore conclude that in the range $1.2 \leqslant \alpha \leqslant 1.3$, a transition occurs in the behavior of the Lyapunov exponent. The value of α, at which the transition happens, depends slightly on the frequency ω. According to our numerical data, the transition appeared at $\alpha = 1.2$ for ω_1 and at $\alpha = 1.24$ for ω_2 (see the inset in Fig. 5, showing the Lyapunov exponents normalized by their maxima). Moreover, no appreciable dependence on the lattice length is observed in this regime. Although it seems plausible that γ vanishes below $\alpha = 1$, the origin of the peak is not clear. A possibility is that sample-to-sample fluctuations become so important that averaging over a much larger ensemble of lattices would be required.

B. Eigenfunctions

Moreover, it is interesting to look at eigenfunctions of a Lévy-type disordered system. In general, spatial part of the frequency-dependent solutions of Eq. (1) can be obtained by solving

$$(\boldsymbol{K} + \omega^2 \boldsymbol{\Lambda})\mathbf{u} = 0, \tag{22}$$

where $\boldsymbol{\Lambda}$ is the diagonalized mass matrix $\boldsymbol{\Lambda} = \mathrm{diag}(m_n)$ and $\boldsymbol{K}$ is the matrix of spring constants expressed by

$$\boldsymbol{K} = \begin{pmatrix} -2k & k & 0 & 0 & \dots \\ k & -2k & k & 0 & \dots \\ 0 & k & -2k & k & \dots \\ \vdots & & & \ddots & \\ 0 & \dots & 0 & k & -2k \end{pmatrix}_{N\times N}.$$

Stationary eigenfunctions of disordered systems can be obtained by numerically solving Eq. (22). For a system with $\alpha = 1.1$ and length $N = 1187$ consisting of $N_d = 200$ defects, eigenfunctions u_n at three different frequencies are presented in Fig. 6. The top panel shows distribution of mass m_n on the entire system which is a step function of $m_n = 1$ or 3. Eigenfunctions of the systems at three different frequencies are depicted in the other panels. According to our results at $\omega = 0.479\,25$ and $\omega = 1.6853$, eigenfunctions are almost extended in a long space between two successive defects. At $\omega = 0.9083$, however, eigenfunctions are localized in a small region inside the system. Note that because of the computational difficulties to diagonalize the system matrix, for this analysis we could only study finite systems with limited number of defects.

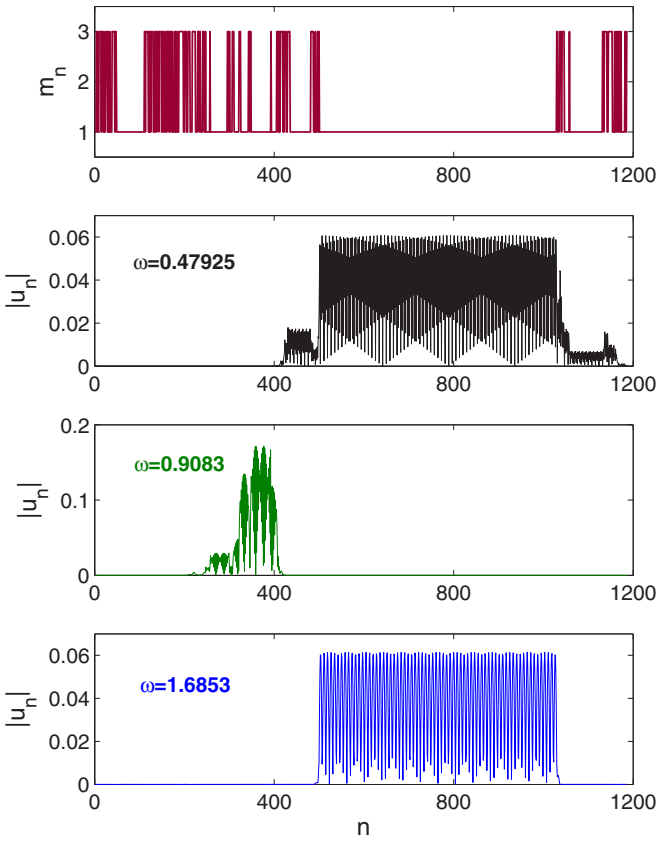

FIG. 6. (Color online) The top panel shows distribution of the mass on a system with $\alpha = 1.1$ and length $N = 1187$ composed of $N_d = 200$ defects (red curve). Other panels (from top to bottom) show eigenfunctions of the system at $\omega = 0.479\,25$ (black curve), $\omega = 0.9083$ (green curve), and $\omega = 1.6853$ (blue curve).

C. Phase dynamics

Next we present our numerical results for the spatial evolution of the phase that, using Eq. (11) and the definition $p_n = q_n - q_{n-1}$, can be computed during the iteration of the transfer matrix by the following relation

$$\theta_n = \tan^{-1}\left(\frac{q_n - q_{n-1}}{\Omega q_n}\right). \tag{23}$$

The computed phase has to be unwrapped to the real axis. The top panel in Fig. 7 illustrates variations of θ_n in systems of equal length $N = 4 \times 10^5$ and different Lévy exponents $\alpha = 1.5, 1.7, 2.5$, at $\omega = 0.1$.

For the statistical analysis, the average drift rate a of the phase ($a \approx \Omega$) was numerically computed and removed by defining $\phi_n = \theta_n - an$. In order to study evolution of ϕ_n over the entire system, the lattice was divided into 50 sublattices of length $n_s = 8 \times 10^3$. For each sublattice, the quantity $(\phi_n - \phi_1)^2$, where $n = 1,..,n_s$ was computed. Averaged over all the sublattices, evolution of the rms phase $\langle\phi_n^2\rangle$ was consequently obtained as shown in the bottom panel of Fig. 7. According to the data, growth of $\langle\phi_n^2\rangle$ is faster in systems with smaller values of α. This can be explained by the fact that disorder fluctuations become stronger, which is in agreement with the superdiffusive behavior of the corresponding random-walk problem [13].

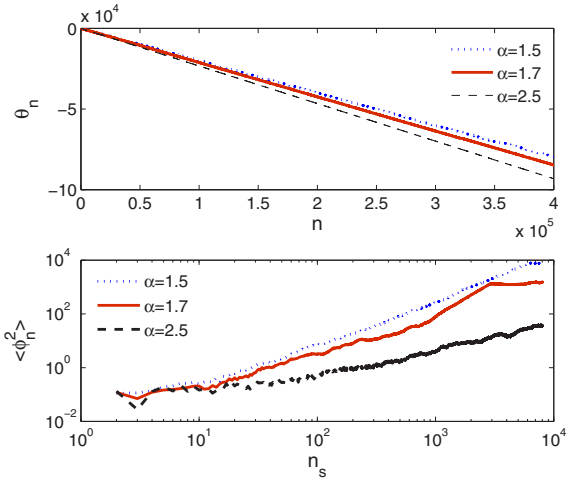

FIG. 7. (Color online) The top panel shows variations of the unwrapped phase θ_n versus n for three different systems with $\alpha = 1.5, 1.7, 2.5$ and length $N = 4 \times 10^5$ at a fixed frequency $\omega = 0.1$. In the bottom panel, variations of $\langle\phi_n^2\rangle$ over a sublattice of length $n_s = 8 \times 10^3$ are presented and compared for the studied systems. Note that $\Omega_{1.5} = 0.1297$, $\Omega_{1.7} = 0.1329$, and $\Omega_{2.5} = 0.1383$, respectively.

IV. EVOLUTION OF WAVE PACKETS

In this section, we investigate the consequences of the above results on the spreading of an initially localized perturbation on an infinite lattice. Although every single eigenstate is exponentially localized, the wave propagation can be nontrivial as low-frequency states form a continuum with arbitrarily large localization lengths.

The starting point of this analysis is a Hamiltonian formulation of the system

$$H = \sum_n \left[\frac{P_n^2}{2m_n} + \frac{1}{2}k(u_{n+1} - u_n)^2\right], \tag{24}$$

where u_n and P_n are displacement and momentum of the mass m_n, respectively. From the Hamiltonian, time evolution of any excitation of interest can be derived. Evidently, local energy at each site of the lattice at time t can be written as

$$e_n(t) = e_n^{\rm kin}(t) + e_n^{\rm pot}(t), \tag{25}$$

$$e_n^{\rm kin}(t) = \tfrac{1}{2}m_n\dot{u}_n(t)^2, \tag{26}$$

$$e_n^{\rm pot}(t) = \tfrac{1}{2}k[u_n(t) - u_{n-1}(t)]u_n(t) - \tfrac{1}{2}k[u_{n+1}(t) - u_n(t)]u_n(t), \tag{27}$$

where $e_n^{\rm kin}(t)$ and $e_n^{\rm pot}(t)$ represent kinetic and potential energies, respectively. Together with the equation of motion [Eq. (5)], these relations constitute the set of governing equations of one-dimensional linear discrete systems.

In our analysis, disordered lattices of length $N = 8 \times 10^3$ with an excitation at the center $n_0 = N/2$ were studied. Two different types of excitation were applied: (i) displacement excitation with $u_n(0) = A\delta_{n,n_0}$ and $P_n(0) \equiv 0$; (ii) momentum excitation with $P_n(0) = B\delta_{n,n_0}$ and $u_n(0) \equiv 0$. As is known, these classes of initial condition yield different asymptotic

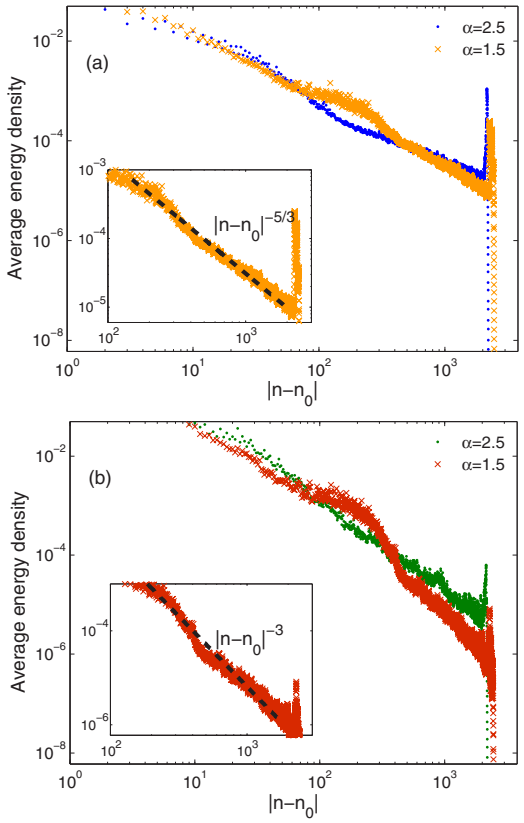

FIG. 8. (Color online) Spreading of the energy density after $t = 3 \times 10^3$ averaged over 2×10^3 realizations. Results are comparisons for two systems with equal lengths $N = 8 \times 10^3$ but different Lévy exponents $\alpha = 1.5$,2.5 with an excitation at $n_0 = N/2$. (a) Momentum excitation with $B = 2$. In the inset, obtained energy density data of the system with $\alpha = 1.5$ are fitted by $|n - n_0|^{-5/3}$ in the asymptotic regime. (b) Displacement excitation with $A = 2$. In the inset, obtained energy density data of the system with $\alpha = 1.5$ are fitted by $|n - n_0|^{-3}$ in the asymptotic regime.

properties due to the fact that the mode energy distribution is different in the two cases [26]. Based on the conservative dynamics of the system and by using a fourth-order symplectic algorithm [27], the set of coupled governing equations were numerically solved. We mainly focused on lattices with $\alpha = 1.5$ and $\alpha = 2.5$ to enable comparison of the two different regimes of transport. Note that the number of defects N_d on the considered lattices were different as N was kept fixed. Obtained results were then averaged over 2×10^3 realizations. Figure 8 presents spread of the averaged energy density over the two systems after $t = 3 \times 10^3$ for both momentum and displacement excitations. In addition to a faster spread of energy, a broadening appeared around the excitation for the system with $\alpha = 1.5$.

Following the analytical approach of Ref. [28] and assuming the frequency-dependent localization length as $\xi_\alpha(\omega) \propto \omega^{-\alpha}$ in the small-frequency regime ($\omega \to 0$), the time- and disorder-averaged energy in a Lévy-type disordered system for a displacement excitation can be written as

$$\langle \overline{e_n(t)} \rangle \propto \int_0^\infty \omega^{2+\alpha} e^{-|n-n_0|\omega^\alpha} d\omega, \tag{28}$$

which asymptotically decays as $|n - n_0|^{-(1+3/\alpha)}$. For a momentum excitation, $\langle \overline{e_n(t)} \rangle$ can be similarly described by

$$\langle \overline{e_n(t)} \rangle \propto \int_0^\infty \omega^{\alpha} e^{-|n-n_0|\omega^\alpha} d\omega, \tag{29}$$

with asymptotic behavior as $|n - n_0|^{-(1+1/\alpha)}$. The insets in Fig. 8 show that our numerical results are consistent with the analytical predictions of the α-dependent power-law decay, at least in the region far enough from the initial excitation. Actually, some sizable deviations at a shorter scale are observed, which are presumably due to the subleading terms neglected in the estimation of Eqs. (28) and (29). In the case of momentum excitation, data for $\alpha = 1.5$ are fitted by $|n - n_0|^{-5/3}$ with a goodness of 95%, as shown in the inset in Fig. 8(a). For the displacement excitation, data for $\alpha = 1.5$ are fitted by $|n - n_0|^{-3}$ with a goodness of 95%, which is illustrated in Fig. 8(b).

Moreover, another interesting entity is time evolution of the moments of the Hamiltonian, which can be defined as [26,28]

$$m_\nu(t) = \frac{\sum_n |n - n_0|^\nu e_n(t)}{H}, \tag{30}$$

where ν is a positive number and $m_\nu(t)$ represents the νth moment of the Hamiltonian at time t. The second moment quantifies degree of the spreading of the wave packet.

In Fig. 9, time evolution of different moments $\langle m_\nu(t) \rangle$ of a wave packet are shown and compared for the two systems. Beyond the clear signature of the growth of the disorder-averaged moments over time, it was observed that around $t \approx 10^3$, the growth exponent suddenly changed in the system with $\alpha = 1.5$. At shorter times, however, we

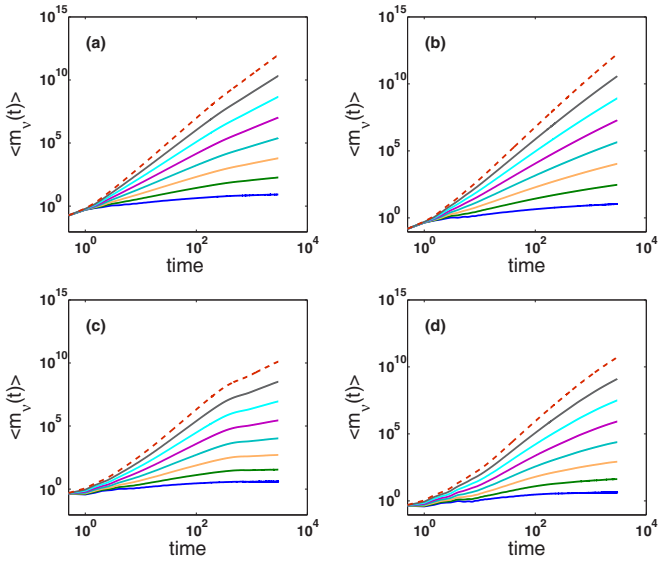

FIG. 9. (Color online) Time evolution of the moments $\langle m_\nu(t) \rangle$ averaged over 2×10^3 realizations for systems with length $N = 8 \times 10^3$. Different colors represent different index ν varying from $\nu = 0.5$ (solid blue line, bottom) to $\nu = 4$ (dashed red line, top) with step $\Delta\nu = 0.5$. Momentum excitation ($B = 2$) was applied at $n_0 = N/2$ on a system with Lévy exponent (a) $\alpha = 1.5$ and (b) $\alpha = 2.5$. Displacement excitation ($A = 2$) was applied at $n_0 = N/2$ on a system with Lévy exponent (c) $\alpha = 1.5$ and (d) $\alpha = 2.5$.

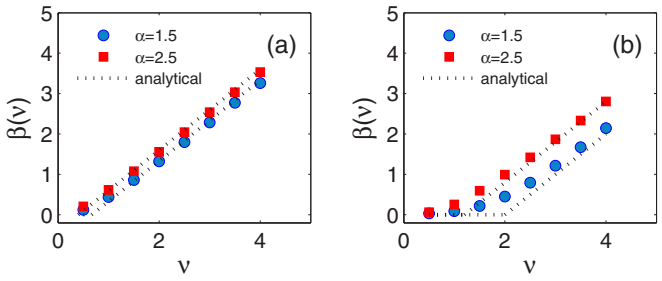

FIG. 10. (Color online) Comparison of $\beta(\nu)$ for the two systems with Lévy exponent $\alpha = 1.5$ (blue circles) and $\alpha = 2.5$ (red squares). Data are obtained by performing power-law fits on $\langle m_\nu(t)\rangle$. Dotted black lines show the numerical solutions of analytical Eqs. (31) and (32) for each system. (a) Momentum excitation ($B = 2$); (b) displacement excitation ($A = 2$).

may assume that correlation effects are not yet strong and the system behaved like a short-range correlated one. Note that such an effect is even more emphasized in the case of displacement excitation. To numerically estimate the scaling of $\langle m_\nu(t)\rangle \propto t^{\beta(\nu)}$, a power-law fit was performed on the averaged moments. The obtained results shown in Fig. 10 reveal that $\beta(\nu)$ is smaller in the system with $\alpha = 1.5$ in comparison with $\alpha = 2.5$.

As already shown and discussed, $\beta(\nu)$ is different in systems with different Lévy parameters. In an effort to determine a general analytic relation for $\beta(\nu,\alpha)$ that describes dependence on both parameters ν and α, the asymptotic forms of Eqs. (28) and (29) were inserted into Eq. (30). Later, by defining an upper cutoff for the summation in the numerator at the ballistic distance $|n - n_0| = ct$, it can be shown that for displacement excitation

$$\beta(\nu,\alpha) = \begin{cases} \nu - \frac{3}{\alpha}, & \alpha\nu > 3, \\ 0, & \alpha\nu < 3, \end{cases} \tag{31}$$

while for momentum excitation

$$\beta(\nu,\alpha) = \begin{cases} \nu - \frac{1}{\alpha}, & \alpha\nu > 1, \\ 0, & \alpha\nu < 1. \end{cases} \tag{32}$$

As shown in Fig. 10, there is an excellent agreement between the theoretical estimates, [according to Eqs. (31) and (32)], and the numerical data obtained by power-law fits on $\langle m_\nu(t)\rangle$ in the long-time regimes.

V. SUMMARY AND CONCLUSION

In this paper, we have studied the localization properties of classical lattice waves in the presence of a power-law correlated disorder. The model is mathematically simple and the choice of the disorder is motivated by the samples known as Lévy glasses [1]. In the first part, we computed frequency-dependent localization length and analyzed how different characteristic parameters can affect it. Using theoretical arguments and numerics, we have shown that in the regime $1 \leqslant \alpha < 2$, $\gamma(\omega) \sim \omega^\alpha$ so that γ mostly decreases as α increases and this trend remains the same even in the regime $\alpha > 2$. The physical interpretation of this result is that, for small frequencies and long wavelengths, the waves see an effective disorder whose fluctuation is scale dependent. More precisely, on distances of the order of the wavelength, the variance of the disorder grows according to some power-law depending on α. In other words, the disorder strength grows upon decreasing α, yielding an anomalous dependence of the localization length on frequency. This is a manifestation of the fact that the disorder is, by construction, scale free.

Large ordered regions can exist inside the system depending on the Lévy exponent α. As expected, we showed that eigenfunctions of the system are localized where the density of disorder is high and extended in the large dilute spaces inside the system. Moreover, due to the superdiffusive nature of the transport in the range $1 \leqslant \alpha < 2$, we showed that the spatial growth of the root-mean-squared phase $\langle \phi_n^2 \rangle$ is greater in systems with smaller values of α.

The anomalous localization properties reflect in the problem of wave packet spreading. An initially localized perturbation attains at large times a characteristic power-law decay as in the uncorrelated case [28,29]. However, in the present case, the exponent of the decay depends on the exponent α of the disorder distribution. This implies that the disorder-averaged momenta $\langle m_\nu(t)\rangle$ must diverge with time, although the initial local energy excitation does not spread completely. The predictions are clearly supported by the numerical results. As a matter of fact, it should be remarked that consideration of $m_2(t)$ alone is not sufficient to conclude that the energy diffuses. Clearly, the origin of such a growth is drastically different from a genuinely (possibly anomalous) diffusive processes observed in nonlinear oscillator chains [30–33] and just stems from the slowly decaying tails.

In the present work we mostly focused on the case $\alpha > 1$. As argued in Sec. II C, the case $\alpha < 1$ should probably correspond to a vanishing Lyapunov exponent. This may indicate that the localization in this regime is not standard. This is further supported by the similarity of the problem with the perturbation growth in strongly intermittent dynamical systems, which indeed yields a vanishing Lyapunov exponent and a subexponential growth of perturbations [34]. Moreover, the divergence of the variance of the distances should lead to huge sample-to-sample fluctuations. Some preliminary data confirm this expectation, suggesting that this case deserves a more detailed future study.

Finally, a natural question regards the extension to higher dimensions. Provided one is able to extend the definition of disorder, we expect the problem to be considerably more difficult in view of the nature of the predicted essential singularity of the localization length at vanishing frequencies [25].

ACKNOWLEDGMENTS

Authors wish to thank Mario Mulansky for assistance with the manuscript and are grateful for the financial support from the European Research Council (FP7/2007-2013), ERC Grant No. 291349.

[1] P. Barthelemy, J. Bertolotti, and D. S. Wiersma, Nature (London) **453**, 495 (2008).
[2] J. Bertolotti, K. Vynck, L. Pattelli, P. Barthelemy, S. Lepri, and D. S. Wiersma, Adv. Funct. Mater. **20**, 965 (2010).
[3] P. W. Anderson, Phys. Rev. **109**, 1492 (1958).
[4] P. Sheng, *Introduction to Wave Scattering, Localization and Mesoscopic Phenomena* (Springer Verlag, Berlin, 2006), Vol. 88.
[5] F. Falceto and V. A. Gopar, Europhys. Lett. **92**, 57014 (2010).
[6] A. A. Fernández-Marín, J. A. Méndez-Bermúdez, and V. A. Gopar, Phys. Rev. A **85**, 035803 (2012).
[7] P. R. Wells, Jr., J. d'Albuquerquee Castro, and S. L. A. de Queiroz, Phys. Rev. B **78**, 035102 (2008).
[8] A. Iomin, Phys. Rev. E **79**, 062102 (2009).
[9] H. Matsuda and K. Ishii, Prog. Theor. Phys. Suppl. **45**, 56 (1970).
[10] E. Barkai, V. Fleurov, and J. Klafter, Phys. Rev. E **61**, 1164 (2000).
[11] C. W. J. Beenakker, C. W. Groth, and A. R. Akhmerov, Phys. Rev. B **79**, 024204 (2009).
[12] P. Barthelemy, J. Bertolotti, K. Vynck, S. Lepri, and D. S. Wiersma, Phys. Rev. E **82**, 011101 (2010).
[13] R. Burioni, L. Caniparoli, and A. Vezzani, Phys. Rev. E **81**, 060101 (2010).
[14] P. Buonsante, R. Burioni, and A. Vezzani, Phys. Rev. E **84**, 021105 (2011).
[15] P. Bernabó, R. Burioni, S. Lepri, and A. Vezzani, Chaos Solitons Fractals **67**, 11 (2014).
[16] L. Devroye, *Non-uniform Random Variate Generation* (Springer-Verlag, New York, 1986).
[17] T. Geisel, in *Lévy Flights and Related Topics in Physics* (Springer, Berlin, 1995), pp. 151–173.
[18] F. A. B. F. de Moura, M. D. Coutinho-Filho, E. P. Raposo, and M. L. Lyra, Phys. Rev. B **68**, 012202 (2003).
[19] A. Costa and F. De Moura, J. Phys.: Condens. Matter **23**, 065101 (2011).
[20] A. Crisanti, G. Paladin, and A. Vulpiani, *Products of Random Matrices* (Springer, Berlin, 1993).
[21] B. Derrida and E. Gardner, J. Phys. (Paris) **45**, 1283 (1984).
[22] F. Izrailev, S. Ruffo, and L. Tessieri, J. Phys. A: Math. Gen. **31**, 5263 (1998).
[23] F. Izrailev, A. Krokhin, and N. Makarov, Phys. Rep. **512**, 125 (2012).
[24] I. F. Herrera-González, F. M. Izrailev, and L. Tessieri, Europhys. Lett. **90**, 14001 (2010).
[25] S. John and M. J. Stephen, Phys. Rev. B **28**, 6358 (1983).
[26] P. K. Datta and K. Kundu, Phys. Rev. B **51**, 6287 (1995).
[27] R. I. McLachlan and P. Atela, Nonlinearity **5**, 541 (1992).
[28] S. Lepri, R. Schilling, and S. Aubry, Phys. Rev. E **82**, 056602 (2010).
[29] P. L. Krapivsky and J. M. Luck, J. Stat. Mech. (2011) P02031.
[30] G. S. Zavt, M. Wagner, and A. Lütze, Phys. Rev. E **47**, 4108 (1993).
[31] P. Cipriani, S. Denisov, and A. Politi, Phys. Rev. Lett. **94**, 244301 (2005).
[32] L. Delfini, S. Denisov, S. Lepri, R. Livi, P. K. Mohanty, and A. Politi, Eur. Phys. J. Spec. Top. **146**, 21 (2007).
[33] M. Mulansky and A. Pikovsky, Europhys. Lett. **90**, 10015 (2010).
[34] P. Gaspard and X. J. Wang, Proc. Natl. Acad. Sci. USA **85**, 4591 (1988).